Electrochemical properties of B-site non-stoichiometric layered perovskite $SmBa_{0.5}Sr_{0.5}Co_xO_{5+d}$ (x=1.9~2.1) cathodes for IT-SOFC

Ji Min Im [a,b], Harald Schlegl [c], Jun-Young Park [d], Seung-Wook Baek [e], Jung Hyun Kim [a,*]

[a] Department of Advanced Materials Science and Engineering, Hanbat National University, 125, Dongseo-Daero, Yuseong-Gu, Daejeon, 34158, Republic of Korea

[b] Fuel Cell Innovations Co., Ltd. 41-7, Techno 11-ro, Yuseong-gu, Daejeon, Republic of Korea

[c] Physics Department, Lancaster University, Bailrigg, Lancaster, LA1 4YB, United Kingdom

[d] HMC, Department of Nanotechnology and Advanced Materials Engineering, Sejong University, Seoul, 05006, Republic of Korea

[e] Interdisciplinary Materials Measurement Institute, Korea Research Institute of Standards and Science (KRISS), 267, Gajeong-Ro, Yuseong-Gu, Daejeon, 34113, Republic of Korea

Corresponding author:*

Jung Hyun Kim: jhkim2011@hanbat.ac.kr, jhkim1870@gmail.com,

Tel: +82-42-821-1239, Fax: +82-42-821-1592,

Department of Advanced Materials Science and Engineering, Hanbat National University, 125, Dongseo-Daero, Yuseong-Gu, Daejeon, 34158, Republic of Korea

Abstract

In this study, layered perovskites were synthesized using a non-stoichiometric synthesis strategy that allowed the variation of the amount of Co substitution in the basic composition of $SmBa_{0.5}Sr_{0.5}Co_2O_{5+d}$ (SBSCO), used as a cathode material for Intermediate Temperature-operating Solid Oxide Fuel Cells (IT-SOFCs).

$SmBa_{0.5}Sr_{0.5}Co_xO_{5+d}$ (x=1.9~2.1, SBSCO-1.9~2.1), B-site non-stoichiometric layered perovskites, were analyzed to characterize the electrical and electrochemical properties with respect to the Co substitution. Among them, $SmBa_{0.5}Sr_{0.5}Co_{2.05}O_{5+d}$ (SBSCO-2.05) exhibited the best electrical and electrochemical properties with an ASR of 0.082 Ωcm^2 and an electrical conductivity of 268.42 S/cm at 700 ºC (measured in air within a series of measurements of increasing measuring temperature). Therefore, B-site non-stoichiometric perovskite compositions with increased Co substitution on their B sites represent a key strategy for achieving high performance cathodes compared to cathodes with stoichiometric compositions.

Keywords: Layered Perovskite, Cathode, Non-Stoichiometric composition, Electrical Conductivity, Microstructure

Highlight

● Layered perovskites with controlled non-stoichiometric compositions achieved by variation of the Co amount at their B-site were selected.

● $SmBa_{0.5}Sr_{0.5}Co_{2.05}O_{5+d}$ shows the lowest ASR of 0.082 Ωcm^2 at 700 ^oC.

● $SmBa_{0.5}Sr_{0.5}Co_{2.05}O_{5+d}$ shows the highest electrical conductivity of 268.42 S/cm at 700 ^oC.

● Non-stoichiometric compositions with increased Co substitution can enhance both electrochemical and electrical properties.

1. Introduction

A solid oxide fuel cell (SOFC) is a device that directly converts chemical energy into electrical energy. It serves as an environmentally friendly power generation device utilizing hydrogen and oxygen as chemical fuels to generate electricity without carbon emissions [1-3]. From the aspects of SOFC operating conditions, SOFCs operate at high temperatures between 600 °C and 1000 °C, which gives them the advantage of offering the highest power conversion efficiency and power density of all conventional fuel cells [4-6]. In addition, operating at high temperatures makes it possible to promote the reaction without requiring expensive catalysts, unlike low-temperature fuel cells. Since they do not use a liquid electrolyte, they have the advantage of not having the problem of electrolyte loss compensation [7].

On the other hand, the benefits of operating in a high temperature range can sometimes come with drawbacks, such as chemical and physical instability between key components and thermal degradation, which can reduce the stability and performance of single cells and stacks [8-10].

Therefore, intermediate temperature-operating SOFCs (IT-SOFCs) with a lower operating temperature range of 500 ºC to 700 ºC are being studied. IT-SOFCs can overcome the problems that occur at high temperatures and offer the benefits of reducing system operating costs and increasing the lifetime of the stack [11]. However, IT-SOFCs have a drawback in that the resistance of each component increases as the operating temperature decreases, especially the polarization resistance of the cathode, which increases significantly by over 50 % of the total resistance [12, 13]. This means that developing an excellent cathode is important to improve the performance of IT-SOFCs.

Consequently, studying the cathodes with layered perovskite structures has been actively underway to achieve high catalytic activity properties for the oxygen reduction reaction (ORR). Layered perovskites with an $AA'B_2O_{5+d}$ structure are characterized by the ordering of the A-

site cations and have a layered structure with $[BO_2]$-[AO]-$[BO_2]$-[AO] layers stacked along the c-axis [14]. This layered structure has the advantage of reducing the oxygen binding strength of the [AO] layer and providing disordered ionic transport channels, which can increase the diffusivity of oxygen ions and cause excellent surface properties [15-19].

A study of performance based on A-site substituents in layered perovskite showed that amongst $LnBaCo_2O_{5+d}$ (Ln=La, Pr, Nd, Sm, Gd, and Y) the perovskites with Sm as A-site cation (SBCO) exhibited excellent electrical performance of 570 S/cm at 200 ºC, and a 1:1 composite of CGO91 and SBCO was reported to exhibit an ASR value as low as 0.05 Ω cm^2 [20]. Especially, the composition $SmBa_{0.5}Sr_{0.5}Co_2O_{5+d}$ (SBSCO) with simultaneous substitution of Ba and Sr at the A-site exhibits excellent electrical conductivity properties of 427.8 S/cm at 700 ºC and ASR as low as 0.09 Ω cm^2 [21].

Various transition metal elements substituted at the B-site can change the catalytic properties of the cathode, and the most commonly used elements are Cu, Co, Ni, Mn, and Fe. These elements can adopt a range of charge values, resulting in good electrical properties [22]. In particular, the Co-based layered perovskite has disadvantages such as high thermal expansion coefficient and high cost. However, it has the advantage of excellent electrical properties and low ASR due to optimal catalytic properties [23, 24, 27]. For example, the material $LaBaCo_2O_{5+d}$ with Co substitution at the B-site is 457 S/cm at 700 ºC, and $LaBaCuFeO_{5+d}$ with Cu and Fe simultaneous substitution is 93.7 S/cm at 700 ºC [25, 26].

Therefore, in this study, cobalt (Co) was utilized as the transition metal at the B-site, and various layered perovskite compositions of $SmBa_{0.5}Sr_{0.5}Co_xO_{5+d}$ (x=1.9, 1.95, 2, 2.05, and 2.1; Abbreviation: SBSCO-1.9~2.1) were employed to analyze the properties of cathodes with different levels of Co substitution, aiming for their direct application in IT-SOFCs.

2. Experiment

2.1. Phase synthesis

Sm_2O_3 (Alfa Aesar, 99.9%), $BaCO_3$ (Samchun, 99.0%), $SrCO_3$ (Aldrich, 99.9%), and Co_3O_4 (Alfa Aesar, 99.7%) were utilized as the primary raw materials to synthesis $SmBa_{0.5}Sr_{0.5}Co_xO_{5-d}$ layered perovskites. For the traditional solid-state reaction (SSR) method, each raw powder was accurately weighted to the third decimal place for chemical composition, and an agate mortar was used for uniform mixing. During this process, ethanol was added in small amounts to prevent the loss of fine powder and powder scattering.

The mixed material was dried at 78 ºC for 24 hours to evaporate ethanol before proceeding to the first calcination. For the first calcination, a heating rate of 5 ºC per minute was maintained to reach 1000 ºC and then the temperature was held at 1000 ºC for 6 hours. During the first calcination, $BaCO_3$ and $SrCO_3$ were reduced to BaO and SrO, respectively, and a partially single phase was formed simultaneously. The secondary calcination was carried out at 1100 ºC for 8 hours with a heating rate of 5 ºC/min, during which all the unreacted raw material powders were converted into a single phase. After the secondary calcination, the powder was uniformly pulverized to prepare the cathode powder using the SSR method.

2.2. Sample characteristics analysis

2.2.1. Synthesis and X-ray diffraction (XRD)

X-ray diffraction (XRD) analysis was performed to confirm the structural characteristics of the synthesized cathodes. This analysis method provides information on the crystal structure and chemical composition by applying X-rays to the sample and obtaining diffracted X-rays specific to the material. As the peak position and intensity in XRD analysis may vary based on the condition of the sample, the cathode was finely powdered using an agate mortar prior to analysis to ensure precise measurements.

In addition to the synthesized single-phase cathode, a composite cathode, consisting of a mixture of electrolyte and single-phase cathode, was produced for XRD analysis. This XRD analysis aimed to identify the suitable electrolyte, as a secondary phase may emerge during the chemical reaction between the electrolyte and cathode, potentially leading to performance decrease. The composite cathodes with Yttria-stabilized zirconia (YSZ) or $Ce_{0.9}Gd_{0.1}O_{2-d}$ (CGO91) electrolytes were mixed using agate mortar after being weighed in a 1:1 mass ratio. After mixing, three different composite cathodes were fabricated of each of the YSZ/SBSCO and CGO91/SBSCO mix combinations by heat treatment at different temperatures of 900, 1000, and 1100 ºC for 3 hours (heating rate: 5 ºC/min). XRD analysis of the composite cathode reveals the reactivity between the cathode and electrolyte depending on the heat treatment temperature.

The equipment employed for XRD analysis utilized Cu ka radiation (Model D/Max 2500, Rigaku (45 Kv, 200 mA, Cu kα radiation)). XRD analysis was performed in the 2 theta (2θ) range from 10 to 90 º and the data were analyzed using the MDI JADE 6 program.

2.2.2. Thermogravimetric analysis (TGA)

Thermogravimetric Analysis (TGA) is a measurement method that analyzes the weight change in a sample. When maintained at a given temperature ramp rate, the weight changes of the sample can be observed as a function of both temperature and time change.

In this study, a Labsys Evo model was employed, and the analysis was conducted within a temperature range of 50 to 900 ºC with a temperature increase of 5 ºC per minute. To ensure precise measurements, the powders underwent 2 hours of heat treatments at 200 ºC to eliminate any remaining moisture. The TGA analysis enables the accurate measurement of weight changes in the range of 50 to 900 ºC for all compositions.

2.2.3. X-ray photoelectron spectroscopy (XPS) analysis

X-ray photoelectron spectroscopy (XPS) is a method that obtains the surface chemical structure by analyzing the photoelectrons emitted from the surface. Consequently, XPS analysis can be utilized to analyze the chemical bonding state and surface properties.

The selected compositions were processed into fine powders for XPS analysis. For XPS analysis, three compositions were chosen: the stoichiometric composition SBSCO-2, the non-stoichiometric composition SBSCO-1.9 with decreased Co amount as an example for a B-site deficient perovskite, and the non-stoichiometric composition SBSCO-2.05 with increased Co amount as an example for a B-site excess perovskite.

XPS measurements were performed using a Sigma Probe model (Thermo VG Scientific, Al Kα Source). The spectra were obtained across the entire binding energy range (0-1400 eV) and within specific ranges for each element (C_{1s}=275-295 eV, O_{1s}=520-550 eV, Co_{2p}=770-820 eV). After the measurements, the data were analyzed using PeakFit version 4. Each binding energy was calibrated with respect to a C_{1s} peak (284.4 eV), and then the peaks were separated and analyzed using Gaussian and Lorentzian functions.

2.3. Electrochemical property measurements and analysis

A half cell with a cathode coated on the top and bottom of the electrolyte support was fabricated to analyze the electrochemical properties. To prepare the electrolyte support, 2.5 g of CGO91 powder was loaded into a circular metal mold and compressed at a pressure of 2 x 10^3 kg/m^2. The pressed CGO91 pellet was heat treated at 1450 ^oC for 6 hours using a heating rate of 5 ^oC/min.

Screen printing was used to coat the electrolyte support with the cathodes. 5 g of cathode powder, 0.1 g of KD-1 dispersant and 100 ml of acetone used as a solvent were mixed in a Nalgene bottle by ball mill process to fabricate the required cathode ink. At this point, ball

milling was performed at 160 rpm for 24 hours. After removal of the zirconia beads the slurry was stirred at room temperature to prepare a cathode ink. The cathode ink was screen printed on top and bottom of the sintered CGO91 electrolyte. The printed samples were heat treated at 1000 ºC for 1 hour to complete the half cell.

The resistance measurements of the half cell were performed using a multi-channel chemical analyzer (Model nStat, HS Technologies) in the temperature range of 500-900 ºC. The measurements were started at 900 ºC reducing the measurement temperature in decrements of 50 ºC finishing with a measurement at 500 ºC, using a frequency range of 0.05-250000 Hz. The measured resistance was multiplied by the screen-printed cathode area of 0.785 cm^2 to calculate the area specific resistance (ASR).

2.4. Electrical conductivity measurements and analysis

To fabricate dense cathode samples, 2.5 g of cathode powder was pressed into a rectangular metal mold (25 mm x 6 mm x 4 mm) at a pressure of $2x10^3$ kg/m^2. After molding the slabs were sintered by heat treatment at 1100 ºC for 3 hours in an air atmosphere. The dense cathode samples were wound with Pt wires along the voltage and current lines using the DC 4 probe method. Pt paste was additionally applied to contact the Pt wire with the sample. The prepared sample was then connected to a Keithley 2400 source meter and the resistance was measured.

The temperature range was from 50 ºC to 900 ºC, measured in 50 ºC steps. In two series of measurements the temperature was first elevated (from 50 ºC to 900 ºC) and then decreased (from 900 ºC to 50 ºC). Air and nitrogen (N_2) atmospheres were used for the measurements. The current applied to measure the resistance was 0.1 A, 0.5 A, and 1 A.

A second set of conductivity measurements was performed using porous cathode material comparable to a condition used in SOFCs. Unlike the dense cathodes, the porous structure makes it impossible to directly measure the electrical conductivity due to its fragile structure,

so the porous cathodes were applied on top of an electrolyte support using a coating method. Specifically, the method of screen printing a thin layer of cathode ink on the electrolyte was used. To prepare the electrolyte substrate, 9 g of CGO91 electrolyte powder was loaded into a rectangular metal mold (30 mm x 23 mm x 2 mm) and compacted under a pressure of 1.5 x 10^3 kg/m^2. Then, a dense CGO91 electrolyte was produced by heat treatment at 1450 ^oC for 6 hours. Cathode ink was screen printed onto the sintered CGO91 electrolyte, and voltage and current lines were printed onto the cathode layer using Pt paste by the DC 4 probe method. The printed samples were then heat treated at 1000 ^oC for 3 hours.

Carefully choosing the applied current values is important because cathodes with a porous microstructure have a lower conductivity than those with a dense microstructure. The respective applied current values were 0.05, 0.075, 0.1, and 0.3 A for air atmosphere and 0.01, 0.02, 0.03, 0.04, and 0.05 A for N_2 atmosphere. The reason for setting a lower current value for a porous microstructure than a dense microstructure is as follows. Porous microstructure cathodes have a lower conductivity than cathodes with a dense microstructure due to their many porosities. Therefore, high current values can cause overvoltage and destroy the porous cathode. The reason for the different current application values between conductivity measurements of cathodes with a porous microstructure in air and N_2 atmospheres is similar. The effect of a N_2 atmosphere and related low oxygen partial pressure on a P-type conductor is a further decrease of conductivity. Overvoltage and destruction of the cathode can occur at lower current values compared to measurements in air atmosphere. The choice of the current range for the measurements aims to avoid overvoltage and destruction while at the same time provide currents high enough for optimal measurement conditions [28].

The measurement equipment and temperature range are the same as those used for measuring electrical conductivity of the dense cathodes, also the method for calculating the electrical conductivity is the same. However, since it is difficult to measure the thickness of the screen-

printed cathode layer directly, a scanning electron microscope (SEM) was used to obtain detailed information about the thickness of the cathode layer.

3. Results and discussion

3.1. Phase synthesis characteristics

3.1.1. X-ray diffraction (XRD)

In Figure 1, all compositions SBSCO-1.9 to 2.1 display characteristic layered perovskite peaks at 23, 33, 41, 47, 59, 69, and 78 °, indicative of an orthorhombic crystal structure, as evidenced by the peak splitting observed at 23, 47, and 59 ° [20, 29-31]. However, in the case of SBSCO-1.9 and SBSCO-1.95, it was observed that during the synthesis process, a secondary phase, identified as $Sr_3Co_2O_{6.13}$ (JCPDS #83-0375) by the peaks (▼) at 24.68, 27.08, 32.3, 43.42, and 45.1 ° in the XRD patterns, occurred. These results indicate that secondary phases appear in non-stoichiometric compositions with less Co substitution compared to stoichiometric compositions. Therefore, SBSCO-2, 2.05, and 2.1 are compositions in which a single phase can be synthesized.

After analyzing the synthesis properties, the electrolyte and cathode were mixed in a 1:1 mass ratio and heat treated for 3 hours at 900 ºC, 1000 ºC, and 1100 ºC, respectively to investigate the chemical reactivity of the electrolyte and cathode as a function of heat treatment temperature. YSZ and CGO91 were used as electrolyte materials. These materials are commonly employed in SOFCs as electrolytes, with YSZ known for high-temperature stability. Furthermore, CGO91 exhibits excellent ionic conductivity even at relatively low temperatures, making it suitable as an electrolyte for IT-SOFCs [32-35].

The XRD results of the composite cathodes with YSZ and CGO91 are shown in Figure 2. In Figure 2. (a), the XRD results of the heat treatment of composite SBSCO-2.05 with CGO91 composite showed that no additional peaks appeared, which indicates that SBSCO-2.05 and

CGO91 do not react at 900 ºC, 1000 ºC, and 1100 ºC. On the other hand, secondary phases such as $SrZrO_3$ (JCPDS #23-0561), Co_3O_4 (JCPDS #43-1003), $Sm_2Zr_2O_7$ (JCPDS #24-1012), and Y_2O_3 (JCPDS #43-0661) occurred when SBSCO-2 and SBSCO-2.05 were heat treated in composite with YSZ, as shown in Figures 2. (b) and 2. (c) respectively. For example, SBSCO-2, when mixed with YSZ, exhibited secondary phases such as $SrZrO_3$, Co_3O_4, and $Sm_2Zr_2O_7$ at all temperatures of 900 ºC, 1000 ºC, and 1100 ºC. Similarly, SBSCO-2.05 showed secondary phases including $SrZrO_3$, Co_3O_4, and $Sm_2Zr_2O_7$ at 900 ºC, and additional peaks of another secondary phase identified as Y_2O_3 when heat treated at 1000 ºC and 1100 ºC. Therefore, to use the electrolyte with the cathode applied in this study, either CGO91 electrolyte should be used, or a buffer layer should be used on top of the YSZ electrolyte to prevent the occurrence of secondary phases through chemical reactions.

In addition, relative intensity of the secondary phase peaks was calculated to accurately analyze the number and concentration of secondary phases in the YSZ/SBSCO composite cathode. Relative intensity is the ratio of the main peak of each secondary phase peak to the YSZ peak (2θ=30.2 º), which is the main peak of the YSZ phase in the composite cathode and is set to 100 %. The main peak positions of secondary phases such as $SrZrO_3$, Co_3O_4, $Sm_2Zr_2O_7$, and Y_2O_3, can be observed at 30.220 º, 36.845 º, 29.257 º, and 29.409 º, respectively [36]. The results of the calculated relative intensities are shown in Figure 2. (d) and Table 1.

Figure 2. (d) illustrates the number and concentration of secondary phases generated by the reaction of SBSCO-2 and SBSCO-2.05 with YSZ with respect to the different temperatures of the heat treatment. For example, when SBSCO-2 and YSZ are reacted, the secondary phase of Y_2O_3 does not occur at all temperatures, and the concentration of $SrZrO_3$ and Co_3O_4 increases with increasing heat treatment temperature, while the concentration of $Sm_2Zr_2O_7$ decreases at 1100 ºC. When SBSCO-2.05 was mixed with YSZ, no secondary phase of Y_2O_3 was observed at 900 ºC, while Y_2O_3 occurred at 1000 ºC and 1100 ºC. In addition, the concentration of all

secondary phases increases with increasing temperature, and the concentration of the secondary phase $Sm_2Zr_2O_7$ increases markedly at 1000 ºC and 1100 ºC. Finally, the higher concentration and number of secondary phases observed in SBSCO-2.05 compared to SBSCO-2 imply that SBSCO-2.05 exhibits a higher chemical reactivity with YSZ.

3.1.2. Thermogravimetric analysis (TGA)

Figure 3. (a) shows the results of thermogravimetric analysis (TGA) to show the change of thermogravimetric weight with temperature for SBSCO formulations with different substitution amounts of Co. Figure 3. (b) shows graphs depicting the change in oxygen content (d) of the different layered perovskite formulations. These calculated values are derived from the equation: $\frac{\text{Formula weight} \times 1.4}{15.9994 \times 100}$. Even though the general chemical formula for the layered perovskites is $SmBa_{0.5}Sr_{0.5}Co_xO_{5+d}$, the average amount of oxide ions in a unit cell of the layered perovskites is far higher than 5. To obtain the average amount of oxide ions in a unit cell of the layered perovskites at RT, the charge states of Sm, Ba, Sr, Co, and O are considered to be +3, +2, +2, +3, and -2. According to standard stoichiometry, their chemical compositions at RT are considered to be $SmBa_{0.5}Sr_{0.5}Co_2O_{5.5}$ for SBSCO-2. The average amount of oxide ions can be increased or decreased depending on the change in thermogravimetric weight according to the TGA analysis in Figure 3. (a) [38]. For example, the average number of oxide ions per unit cell in the SBSCO-2.05 composition is about 5.575 at RT. Using this value as a starting point and adding 0.047 oxide ions from the TGA indicated weight gain with the rise in temperature from RT to 300 ºC the conclusion for the average oxide ion number per unit cell in SBSCO-2.05 at 300 ºC is around 5.622. Generally, after an increase in oxygen content between RT and 300 ºC the oxygen content is decreased at temperatures higher than 300 ºC by the formation of oxygen vacancies in the lattice, the difference in oxygen content between the values of room temperature and the values at higher temperatures are denoted as d (see Table

2), this d-value can function as an indicator of how many oxygen vacancies have formed in the perovskite lattice during the process of heating above 300 ºC. Using the thermogravimetric results in Figure 3. (a), the decrease in oxygen content (d) in the layered perovskite was calculated and summarized in Figure 3. (b). As shown in Figure 3. (a), a decrease in the weight with increasing temperature is evident for all compositions, with a particularly significant decrease at 300 ºC. This decrease indicates that the generation of oxygen vacancies in the lattice occurs at temperatures above 300 ºC [20]. The calculated decrease in oxygen content d (creation of oxygen vacancies) by composition are summarized in Table 2.

Figure 3 and Table 2 show that, with the exception of SBSCO-1.95, the weight loss at high temperature is proportional to the increase in Co substitution. This shows that the amount of oxygen vacancies created with rising temperature increases as the amount of Co substitution increases. Therefore, the amount of oxygen vacancies per unit cell created in SBSCO-2.1 is 0.59 at 900 ºC, which is the largest amount of oxygen vacancies in all compositions. The oxygen content can also affect the electrical and electrochemical performance, the reason for this is discussed in the following sections 3.2 and 3.3.

3.2. Electrochemical characteristics

The electrochemical properties as a function of the amount of Co substitution are shown in Figure 4 and Table 3. As shown in Figure 4. (a), the ASR values of SBSCO-1.9 to 2.1 at 700 ºC were found to be 0.16, 0.13, 0.18, 0.08, and 0.12 Ωcm^2, respectively. It is noteworthy that SBSCO-2.05 exhibited the lowest ASR among them. Moreover, the activation energy of SBSCO-2.05 was calculated to be 0.985 eV, showing that it is the lowest among the different compositions. When comparing the electrochemical performance through the ASR values of all the compositions, the stoichiometric composition SBSCO-2 shows the highest ASR values. Both B-site deficient layered perovskites SBSCO-1.9 and SBSCO-1.95 and B-site excess

layered perovskites SBSCO-2.05 and SBSCO-2.1 with Co non-stoichiometric compositions have enhanced electrochemical properties compared to the stoichiometric layered perovskite SBSCO-2.

In particular, the SBSCO-2.05 composition exhibits the most excellent electrochemical properties. This observation can be correlated with the XPS analysis shown in Figure 5. The O_{1s} spectra of SBSCO-2 and SBSCO-2.05 are shown in Figure 5. (a, b), and Table 5. High binding energy (HBE) is related to the surface properties that oxygen molecules can adsorb [37, 39-41]. The area % values of the HBE corresponding to SBSCO-2 and SBSCO-2.05 are determined to be 78.96 % and 80.19 %, respectively. The higher HBE area % in SBSCO-2.05 indicates advanced electrochemical characteristics (=lower ASR characteristics).

The electrochemical properties can also be assessed by examining the TGA results depicted in Figure 3. In Figure 3. (b), the generation of oxygen vacancies varies with the Co substitution level, as the amount of Co substitution increases, a significant number of oxygen vacancies are generated, enhancing the Oxygen Reduction Reaction (ORR) characteristics. However, an excessive concentration of oxygen vacancies caused by defects can impede oxygen mobility by scattering oxygen vacancies, thereby reducing ORR properties [44]. Therefore, among the compositions ranging from SBSCO-1.9 to 2.1, SBSCO-2.05 exhibits the best electrochemical properties.

Electrochemical impedance spectroscopy (EIS) allows the division of the total resistance into ohmic resistance and polarization resistance and furthermore the distinction between high frequency and low frequency parts of the polarization resistance. Polarization resistance occurring at a high frequency ($2.5x10^5$ Hz to 1 Hz) is denoted as R_1, signifying the resistance encountered as oxygen ions migrate from the cathode interface into the electrolyte. Polarization resistance occurring at a low frequency (1 Hz to 0.05 Hz) is denoted as R_2, signifying the adsorption of oxygen molecules on the cathode and their diffusion into the cathode [42]. The

R_1 and R_2 values of an EIS of all SBSCO compositions are depicted in Figure 4. (b) for measuring temperatures between 600 ºC and 900 ºC enabling us to identify the rate determining step (RDS) of the ORR reaction. R_1 exhibits a significantly larger value than R_2 for all samples and at all measuring temperatures. For example, SBSCO-2.05 at 700 ºC shows an R_1 value of 0.076 Ωcm^2 and an R_2 value of 0.006 Ωcm^2. Consequently, the RDS of all samples is determined by R_1, the resistance that occurs when oxygen ions move from the cathode interface into the electrolyte.

Figure 4. (b) and Table 4 present the fitted impedance results for SBSCO-2.05, which has the lowest ASR values. The values of R_1 are larger than those of R_2 at all measured temperatures. Therefore, the ASR characteristics of SBSCO-2.05 are dependent on R_1, but the relative ratio of R_2 increased within the temperature range from 600 ºC to 900 ºC. In other words, at the low temperature of 600 ºC, the value of R_1 constitutes a larger proportion of the total resistance, whereas at the high temperature of 900 ºC, the values of R_1 and R_2 are similar. This implies that the resistance of oxygen ions moving into the electrolyte at the cathode interface is similar to the resistance caused by the adsorption of oxygen molecules and their movement in the cathode bulk if the sample is measured at a temperature of 900 ºC.

The ASR values and activation energy of the composite cathode (SBSCO-2.05 with CGO91) are compared to that of the SBSCO-2.05 single phase in Figure 4. (a). Both the ASR values and the activation energy of the composite cathode are decreased compared to that of the SBSCO-2.05 single phase. This indicates that the addition of CGO91 effectively decreases the resistance of the cathode by expanding the triple phase boundary (TPB) [43]. For example, comparing the ASR values of SBSCO-2.05 single-phase and of the CGO91/SBSCO-2.05 composite at various temperatures, the ASR of single-phase SBSCO-2.05 at 600, 700, and 800 ºC is 0.499 Ωcm^2, 0.082 Ωcm^2, and 0.032 Ωcm^2, while the ASR of the CGO91/SBSCO-2.05 composite is 0.257 Ωcm^2, 0.052 Ωcm^2, and 0.019 Ωcm^2.

3.3. Electrical conductivities

For all samples with the compositions of SBSCO-1.9~2.1, both dense microstructure (Bar-type samples) and porous microstructure (Porous-type samples) samples were prepared to analyze the electrical conductivity characteristics as a function of their microstructure.

3.3.1. Electrical conductivities of dense microstructure cathodes

The electrical conductivity measurement results of SBSCO-1.9~2.1 with dense microstructure are shown in Figure 6. The measurements of electrical conductivity as a function of temperature were performed varying three main conditions: first, the process involved measuring conductivities during the heat up phase, while increasing the temperature (closed symbol, hereafter Up), but conductivities were also measured during the cool down phase, while decreasing the temperature (open symbol, hereafter Down); second, in different atmospheres, including air (□, square) and N_2 (○, circle); and finally, under applied current conditions of 0.1 A, 0.5 A, and 1 A.

First, when comparing the Up and Down conditions, electrical conductivity values measured in the Down condition are generally higher compared to the electrical conductivity values measured in the Up condition. Measuring the electrical conductivity during the cool down phase after the heat plateau of 900 ºC means that the samples have already gone through sufficient thermal activation, which improves the movability of charge carriers in the cathode [45]. For example, in Figure 6. (a), for SBSCO-1.9 measured under the condition of air atmosphere and 0.1 A, the electrical conductivity values are 216.32 S/cm, 186.43 S/cm, and 157.60 S/cm at 500, 600, and 700 ºC for the Up condition (■) and 241.60 S/cm, 197.87 S/cm, and 163.17 S/cm at 500, 600, and 700 ºC for the Down condition (□). Therefore, the electrical conductivity values are higher for the Down condition.

Secondly, when comparing the conductivities of samples under air and N_2 atmospheres, higher electrical conductivity values can be observed in the air atmosphere, indicating that all samples are typical P-type conductors [45, 46]. For example, in Figure 6. (c) for SBSCO-2, the measured electrical conductivity values under the condition of Up process and 0.1 A are 287.45 S/cm, 240.37 S/cm, and 196.63 S/cm at 500, 600, and 700 ºC for air atmosphere (■), and 227.75 S/cm, 182.01 S/cm, and 144.90 S/cm at 500, 600, and 700 ºC for N_2 atmosphere (●).

Third, a lower current value results in a higher electrical conductivity compared to the conductivity values achieved under a higher applied current. Therefore, among the three applied current values of 0.1 A (black color), 0.5 A (blue color), and 1 A (magenta color), the highest electrical conductivity value is observed at 0.1 A. For example, in Figure 6. (d) for the SBSCO-2.05, measured under the condition of Up process and air atmosphere, the electrical conductivity values are 385.26 S/cm, 326.87 S/cm, 268.42 S/cm at 500, 600, and 700 ºC for the applied current value of 0.1 A (■); 372.75 S/cm, 315.47 S/cm, and 260.52 S/cm at 500, 600, and 700 ºC for the applied current value of 0.5 A (■), and 373.25 S/cm, 314.40 S/cm, and 260.25 S/cm at 500, 600, and 700 ºC for the applied current value of 1 A (■). As mentioned above, the electrical conductivity values at an applied current value of 0.1 A are superior, however, the conductivity values at applied current values of 0.5 A and 1 A are very similar, even if the electrical conductivity values at the applied current value of 0.5 A are slightly higher than those at the applied current value of 1 A. The trend of higher electrical conductivity values at a lower applied current remains consistent. Therefore, with a dense microstructure, a lower applied current value results in a higher electrical conductivity, attributed to difference in the movement of the holes, which serve as the main charge carrier [46-49]. In other words, when a lower current value is applied, the flow of holes increases, which results in a high electrical conductivity characteristic.

Additionally, the conductivities measured during the Down process in N_2 atmosphere (○, ○,

○) under all applied current conditions show the behavior of a semi-conductor with increasing conductivity as the temperature increases. In contrast, excluding the results obtained from the Down process measured under N_2 conditions, under all other conditions it is observed that conductivity decreases with increasing temperature, originating from metallic behavior. This difference in these behaviors can be explained by variations in the atmosphere and the differences in the Up and Down processes. The starting point for all the measurements during the Down process is a high plateau temperature of 900 °C, together with concurrently maintaining N_2 atmosphere this is creating a very low oxygen partial pressure. Under these conditions, all measured P-type samples do not maintain thermal stability due to the high temperature and low oxygen partial pressure, which leads to a change in the surface bonding property [49-51]. Therefore, the behavior changes from metallic to semi-conductor.

The electrical conductivity values for all compositions SBSCO-1.9 to 2.1 were compared in Figure 6. (f) under the conditions of the Up process and in the presence of air, applying the same current value of 0.1 A. The conductivity values of SBSCO-1.9, SBSCO-1.95, SBSCO-2, SBSCO-2.05 and SBSCO-2.1 under these conditions are 157.60 S/cm, 186.21 S/cm, 196.63 S/cm, 268.42 S/cm, and 213.37 S/cm at 700 °C. This indicates that SBSCO-2.05 exhibits the most superior electrical characteristics among them. This superiority in conductivity of SBSCO-2.05 over all other measured SBSCO compositions can be observed at all temperatures, measured at 600, 650, 700, 750, and 800 °C, it consistently shows the same trend in electrical conductivity values.

These electrical properties can be correlated and analyzed with the TGA results in Figure 3. The mobility of charge carriers, holes, is recognized to play a crucial role in determining the electrical characteristics. If the amount of oxygen vacancies generated by increasing the amount of Co substitution is too large, this breaks the Co-O-Co bonds through which these charge carriers move [44], which deteriorates the electrical properties. The decrease in

conductivity at temperatures above 300 ºC, as depicted in Figures 6. (a-e), can be attributed to the rapid generation of oxygen vacancies observed at temperatures above 300 ºC in Figure 3. (b). SBSCO-2.05 exhibits the highest electrical conductivity value despite the increased Co substitution, as can be seen in Figure 6. (f). The composition SBSCO-2.05 seems to inhabit a "sweet spot", an optimal amount of both Co at the B-site of the perovskite and of the number of oxygen and of oxygen vacancies. This is because the existing oxygen content is higher in SBSCO-2.05 due to the chemical composition difference. At the lowest temperatures the oxygen content in SBSCO-2.05 is higher than in most SBSCO compositions, and after increase of temperature, reduction and formation of oxygen vacancies, the final oxygen content of SBSCO-2.05 also has the second largest value of all investigated SBSCO compositions, as shown in Table 2. Despite the occurrence of oxygen vacancies the oxygen content in SBSCO-2.05 remains high enough to leave the Co-O-Co bonds unbroken, enhancing the mobility of holes and contributing to excellent electrical properties.

The outstanding electrical properties of SBSCO-2.05 can also be explained by the XPS analysis results shown in Figure 5. In Figure 5. (c, d) and Table 6, which displays the results of Co_{2p} spectra, the first satellite peak, ranging from 787.36 eV to 787.46 eV, originated from the mixture of Co^{2+} and Co^{4+}, while the second satellite peak, spanning from 804.08 eV to 804.2 eV, is assigned to the interaction of Co^{3+} and Co^{4+} [37, 39, 40]. The area % values of the first satellite peak in SBSCO-2 and SBSCO-2.05 are 6.03 % and 3.9 %, respectively. However, the values of the second satellite peak are 9.76 % and 11.66 %. Consequently, SBSCO-2.05, characterized by a larger coexistence area of Co^{3+} and Co^{4+}, exhibits the highest electrical conductivity value.

3.3.2. Electrical conductivities of cathodes with a porous microstructure

SBSCO-2.05 exhibits the best conductivity values among all the compositions with a dense

microstructure. Therefore, as described at the end of section 2.4., this composition was also prepared as a sample with a porous microstructure to investigate the influence of a porous microstructure on the electrical conductivity of a cathode sample. The electrical conductivity measurement result of the porous-type sample of SBSCO-2.05 is presented in Figure 7.

The dense bar-type sample exhibits metallic behavior in most conditions, whereas the porous-type sample exhibits semi-conductor behavior in all conditions. Additionally, the difference in electrical conductivity values with applied current is significant for the dense bar-type sample, while the porous-type sample does not show a significant difference of conductivity with a different applied current. For example, the porous-type sample exhibits almost the same conductivity value at all applied current levels, as shown in Figure 7. (a, b), because the charge carriers are restricted by the pores within the porous sample under all conditions.

In addition, under the same conditions of air atmosphere, Up process, and 0.1 A, the maximum value of electrical conductivity for the SBSCO-2.05 bar-type sample is 663.42 S/cm at 50 ºC, while the maximum value of electrical conductivity for the porous-type sample is 388.89 S/cm at 900 ºC. The change from a dense microstructure to a porous microstructure results in a discontinuous electrical path due to the density difference and, therefore a decrease in conductivity attributed to the restriction of charge carrier movement [46, 47, 49].

4. Conclusion

In this study, $SmBa_{0.5}Sr_{0.5}Co_xO_{5+d}$ (x=1.9~2.1) with a layered perovskite structure was utilized to characterize the properties of cathodes depending on the amount of Co substitution. Among these compositions, SBSCO-2.05 was identified as a composition that satisfied the conditions for synthesizing a single phase based on XRD analysis, and it was expected to exhibit no performance degradation due to the absence of secondary phases.

It also exhibited the lowest ASR property of 0.082 Ωcm^2 and the lowest activation energy

value of 0.985 eV at 700 ºC due to its excellent surface adsorption property, as evidenced by the highest HBE area % in the O_{1s} spectra of XPS analysis. When composited in a 1:1 ratio with the electrolyte material CGO91, better electrochemical properties of 0.052 Ωcm^2 and 0.832 eV at 700 ºC could be achieved due to an increase in TPB area and little difference in the thermal expansion coefficient.

In the Co_{2p} spectra of the XPS analysis, the highest area % of corresponds to satellite peaks with coexisting Co^{3+} and Co^{4+}, indicating excellent electrical properties. Consequently, the dense microstructure cathode exhibits outstanding electrical conductivity values of 268.42 S/cm at 700 ºC (measured in air).

The excellent electrochemical properties (i.e., low ASR and activation energy) of the material can contribute to the reduced degradation and fast ORR reaction in SOFC cathodes. In addition, the high electrical conductivity values can facilitate the occurrence of the ORR reaction across the entire cathode surface. For all these reasons this study identifies the SBSCO-2.05 composition as the optimal cathode material for an IT-SOFC amongst all studied compositions $SmBa_{0.5}Sr_{0.5}Co_xO_{5+d}$ (x=1.9~2.1). The increased Co substitution compared to the stoichiometric composition SBSCO-2 was identified as the main reason for the superiority of SBSCO-2.05.

Acknowledgments

This research was supported by the research fund of Hanbat National University in 2023

Declaration of competing interest

The authors declare that they have no known competing financial interests or personal relationships that could have appeared to influence the work reported in this paper.

Reference

[1] A.M. Abdalla, S. Hossain, A.T. Azad, P.M.I. Petra, F. Begum, S.G. Eriksson, A.K. Azad, Nanomaterials for solid oxide fuel cells: A review, Renew. Sustain. Energy Rev. 82 (2018) 353–368. https://doi.org/10.1016/j.rser.2017.09.046.

[2] S.J. Davis, N.S. Lewis, M. Shaner, S. Aggarwal, D. Arent, I.L. Azevedo, S.M. Benson, T. Bradley, J. Brouwer, Y.M. Chiang, C.T.M. Clack, A. Cohen, S. Doig, J. Edmonds, P. Fennell, C.B. Field, B. Hannegan, B.M. Hodge, M.I. Hoffert, E. Ingersoll, P. Jaramillo, K.S. Lackner, K.J. Mach, M. Mastrandrea, J. Ogden, P.F. Peterson, D.L. Sanchez, D. Sperling, J. Stagner, J.E. Trancik, C.J. Yang, K. Caldeira, Net-zero emissions energy systems, Science (80-.). 360 (2018). https://doi.org/10.1126/science.aas9793.

[3] Q. Yang, D. Tian, R. Liu, H. Wu, Y. Chen, Y. Ding, X. Lu, B. Lin, Exploiting rare-earth-abundant layered perovskite cathodes of LnBa0.5Sr0.5Co1.5Fe0.5O5+δ (Ln=La and Nd) for SOFCs, Int. J. Hydrogen Energy. 46 (2021) 5630–5641. https://doi.org/10.1016/j.ijhydene.2020.11.031.

[4] S.D. Priya, A.I. Selvakumar, A.S. Nesaraj, Overview on ceramic and nanostructured materials for solid oxide fuel cells (Sofcs) working at different temperatures, J. Electrochem. Sci. Technol. 11 (2020) 99–116. https://doi.org/10.33961/jecst.2019.00612.

[5] J.S. Szmyd, World Energy Resources and New Technologies, Pap. Glob. Chang. IGBP. 23 (2016) 21–35. https://doi.org/10.1515/igbp-2016-0003.

[6] A. V. Nikonov, K.A. Kuterbekov, K.Z. Bekmyrza, N.B. Pavzderin, A brief review of conductivity and thermal expansion of perovskite-related oxides for SOFC cathode, Eurasian J. Phys. Funct. Mater. 2 (2018) 274–292. https://doi.org/10.29317/EJPFM.2018020309.

[7] P. Vinchhi, M. Khandla, K. Chaudhary, R. Pati, Recent advances on electrolyte materials for SOFC: A review, Inorg. Chem. Commun. 152 (2023) 110724. https://doi.org/10.1016/j.inoche.2023.110724.

[8] Y. Du, C. Finnerty, J. Jiang, Thermal Stability of Portable Microtubular SOFCs and Stacks, J. Electrochem. Soc. 155 (2008) B972. https://doi.org/10.1149/1.2953590.

[9] M. Fallah Vostakola, B. Amini Horri, Progress in Material Development for Low-Temperature Solid Oxide Fuel Cells: A Review, Energies. 14 (2021) 1280. https://doi.org/10.3390/en14051280.

[10] D. Fu, F. Jin, T. He, A-site calcium-doped Pr1-xCaxBaCo2O5+δ double perovskites as cathodes for intermediate-temperature solid oxide fuel cells, J. Power Sources. 313 (2016) 134–141. https://doi.org/10.1016/j.jpowsour.2016.02.071.

[11] D.J.L. Brett, A. Atkinson, N.P. Brandon, S.J. Skinner, Intermediate temperature solid oxide fuel cells, Chem. Soc. Rev. 37 (2008) 1568–1578. https://doi.org/10.1039/b612060c.

[12] A. Weber, E. Ivers-Tiffée, Materials and concepts for solid oxide fuel cells (SOFCs) in stationary and mobile applications, J. Power Sources. 127 (2004) 273–283. https://doi.org/10.1016/j.jpowsour.2003.09.024.

[13] S.J. Skinner, Recent advances in perovskite-type materials for solid oxide fuel cell cathodes, Int. J. Inorg. Mater. 3 (2001) 113–121. https://doi.org/10.1016/S1466-6049(01)00004-6.

[14] S. Sun, Z. Cheng, Electrochemical Behaviors for Ag, LSCF and BSCF as Oxygen Electrodes for Proton Conducting IT-SOFC, J. Electrochem. Soc. 164 (2017) F3104–F3113. https://doi.org/10.1149/2.0121710jes.

[15] S. Yoo, S. Choi, J. Kim, J. Shin, G. Kim, Investigation of layered perovskite type $NdBa_{1-x}Sr_xCo_2O_{5+\delta}$ (x = 0, 0.25, 0.5, 0.75, and 1.0) cathodes for intermediate-temperature solid oxide fuel cells, Electrochim. Acta. 100 (2013) 44–50. https://doi.org/10.1016/j.electacta.2013.03.041.

[16] D. Chen, R. Ran, K. Zhang, J. Wang, Z. Shao, Intermediate-temperature electrochemical performance of a polycrystalline $PrBaCo_2O_{5+\delta}$ cathode on samarium-doped

ceria electrolyte, J. Power Sources. 188 (2009) 96–105. https://doi.org/10.1016/j.jpowsour.2008.11.045.

[17] G. Kim, S. Wang, A.J. Jacobson, L. Reimus, P. Brodersen, C.A. Mims, Rapid oxygen ion diffusion and surface exchange kinetics in $PrBaCo_2O_{5+x}$ with a perovskite related structure and ordered a cations, J. Mater. Chem. 17 (2007) 2500–2505. https://doi.org/10.1039/b618345j.

[18] S.H. Woo, K.E. Song, S.-W. Baek, H. Kang, W. Choi, T.H. Shin, J.-Y. Park, J.H. Kim, Pr- and Sm-Substituted Layered Perovskite Oxide Systems for IT-SOFC Cathodes, Energies. 14 (2021) 6739. https://doi.org/10.3390/en14206739.

[19] S.L. Pang, X.N. Jiang, X.N. Li, H.X. Xu, L. Jiang, Q.L. Xu, Y.C. Shi, Q.Y. Zhang, Structure and properties of layered-perovskite $LaBa_{1-x}Co_2O_{5+\delta}$ (x = 0-0.15) as intermediate-temperature cathode material, J. Power Sources. 240 (2013) 54–59. https://doi.org/10.1016/j.jpowsour.2013.04.005.

[20] J.H. Kim, Y. Kim, P.A. Connor, J.T.S. Irvine, J. Bae, W. Zhou, Structural, thermal and electrochemical properties of layered perovskite $SmBaCo_2O_{5+d}$, a potential cathode material for intermediate-temperature solid oxide fuel cells, J. Power Sources. 194 (2009) 704–711. https://doi.org/10.1016/j.jpowsour.2009.06.024.

[21] J.H. Kim, M. Cassidy, J.T.S. Irvine, J. Bae, Electrochemical investigation of composite cathodes with $SmBa_{0.5}Sr_{0.5}Co_2O_{5-\delta}$ cathodes for intermediate temperature-operating solid oxide fuel cell, Chem. Mater. 22 (2010) 883–892. https://doi.org/10.1021/cm901720w.

[22] A. Orera, P.R. Slater, New chemical systems for solid oxide fuel cells, Chem. Mater. 22 (2010) 675–690. https://doi.org/10.1021/cm902687z.

[23] S.S. Hashim, F. Liang, W. Zhou, J. Sunarso, Cobalt-Free Perovskite Cathodes for Solid Oxide Fuel Cells, ChemElectroChem. 6 (2019) 3549–3569. https://doi.org/10.1002/celc.201900391.

[24] A.I. Klyndyuk, M. Mosiałek, D.S. Kharitonov, E.A. Chizhova, M. Zimowska, R.P.

Socha, A. Komenda, Structural and electrochemical characterization of $YBa(Fe,Co,Cu)_2O_{5+\delta}$ layered perovskites as cathode materials for solid oxide fuel cells, Int. J. Hydrogen Energy. 46 (2021) 16977–16988. https://doi.org/10.1016/j.ijhydene.2021.01.141.

[25] R. Pelosato, A. Donazzi, G. Dotelli, C. Cristiani, I. Natali Sora, M. Mariani, Electrical characterization of co-precipitated $LaBaCo_2O_{5+\delta}$ and $YBaCo_2O_{5+\delta}$ oxides, J. Eur. Ceram. Soc. 34 (2014) 4257–4272. https://doi.org/10.1016/j.jeurceramsoc.2014.07.005.

[26] Q. Zhou, T. He, Q. He, Y. Ji, Electrochemical performances of $LaBaCuFeO_{5+x}$ and $LaBaCuCoO_{5+x}$ as potential cathode materials for intermediate-temperature solid oxide fuel cells, Electrochem. Commun. 11 (2009) 80–83. https://doi.org/10.1016/j.elecom.2008.10.035.

[27] R. Pelosato, G. Cordaro, D. Stucchi, C. Cristiani, G. Dotelli, Cobalt based layered perovskites as cathode material for intermediate temperature Solid Oxide Fuel Cells: A brief review, J. Power Sources. 298 (2015) 46–67. https://doi.org/10.1016/j.jpowsour.2015.08.034.

[28] J.M. Im, K.E. Song, H. Schlegl, H. Kang, W. Choi, S.W. Baek, J.Y. Park, H.S. Kim, J.H. Kim, Generation of nanoflowers and nanoneedles on Co-based layered perovskite of IT-SOFC cathode affecting electrical conductivities, Int. J. Hydrogen Energy. 48 (2023) 35229–35239. https://doi.org/10.1016/j.ijhydene.2023.05.327.

[29] J.H. Kim, M. Cassidy, J.T.S. Irvine, J. Bae, Advanced Electrochemical Properties of $LnBa_{0.5}Sr_{0.5}Co_2O_{5+\delta}$ (Ln=Pr, Sm, and Gd) as Cathode Materials for IT-SOFC, J. Electrochem. Soc. 156 (2009) B682. https://doi.org/10.1149/1.3110989.

[30] T. V. Aksenova, L.Y. Gavrilova, A.A. Yaremchenko, V.A. Cherepanov, V. V. Kharton, Oxygen nonstoichiometry, thermal expansion and high-temperature electrical properties of layered $NdBaCo_2O_{5+\delta}$ and $SmBaCo_2O_{5+\delta}$, Mater. Res. Bull. 45 (2010) 1288–1292. https://doi.org/10.1016/j.materresbull.2010.05.004.

[31] J. Marrero-Jerez, J. Peña-Martínez, P. Núñez, Study of the oxygen desorption from $GdBa_{1-x}Sr_xCo_2O_{5+\delta}$ (x = 0, 0.25, 0.5 and 1): Effect of the Sr-content on the oxidation state of

cobalt ions, J. Alloys Compd. 606 (2014) 269–272. https://doi.org/10.1016/j.jallcom.2014.04.021.

[32] C. Brahim, A. Ringuedé, E. Gourba, M. Cassir, A. Billard, P. Briois, Electrical properties of thin bilayered YSZ/GDC SOFC electrolyte elaborated by sputtering, J. Power Sources. 156 (2006) 45–49. https://doi.org/10.1016/j.jpowsour.2005.08.017.

[33] W.S. Jang, S.H. Hyun, S.G. Kim, Preparation of YSZ/YDC and YSZ/GDC composite electrolytes by the tape casting and sol-gel dip-drawing coating method for low-temperature SOFC, J. Mater. Sci. 37 (2002) 2535–2541. https://doi.org/10.1023/A:1015451910081.

[34] S. Cho, Y. Kim, J.H. Kim, A. Manthiram, H. Wang, High power density thin film SOFCs with YSZ/GDC bilayer electrolyte, Electrochim. Acta. 56 (2011) 5472–5477. https://doi.org/10.1016/j.electacta.2011.03.039.

[35] S. Dwivedi, Solid oxide fuel cell: Materials for anode, cathode and electrolyte, Int. J. Hydrogen Energy. 45 (2020) 23988–24013. https://doi.org/10.1016/j.ijhydene.2019.11.234.

[36] X. Gao, H. Ran, Q. Zhou, T. Sekine, J. Liu, Y. Chen, P. Chen, Formation of Novel Bimetal Oxide $In_2V_2O_7$through a Shock Compression Method, ACS Omega. 7 (2022) 27602–27608. https://doi.org/10.1021/acsomega.2c03220.

[37] B.J. Tan, K.J. Klabunde, P.M.A. Sherwood, XPS Studies of Solvated Metal Atom Dispersed Catalysts. Evidence for Layered Cobalt—Manganese Particles on Alumina and Silica, J. Am. Chem. Soc. 113 (1991) 855–861. https://doi.org/10.1021/ja00003a019.

[38] M. Li, W. Zhou, M. Zhao, Z. Zhu, "A comparative study of $SrCo_{0.8}Nb_{0.2}O_{3-\delta}$ and $SrCo_{0.8}Ta_{0.2}O_{3-\delta}$ as low-temperature solid oxide fuel cell cathodes: effect of non-geometry factors on the oxygen reduction reaction", J. Mater. Chem. A. 3 (2015) 24064-24070. https://doi.org/10.1039/C5TA07178J

[39] A. Subardi, C.C. Chen, M.H. Cheng, W.K. Chang, Y.P. Fu, Electrical, thermal and electrochemical properties of $SmBa_{1-x}Sr_xCo_2O_{5+\delta}$ cathode materials for intermediate-

temperature solid oxide fuel cells, Electrochim. Acta. 204 (2016) 118–127. https://doi.org/10.1016/j.electacta.2016.04.069.

[40] Y. Kim, H. Schlegl, K. Kim, J.T.S. Irvine, J.H. Kim, X-ray photoelectron spectroscopy of Sm-doped layered perovskite for intermediate temperature-operating solid oxide fuel cell, Appl. Surf. Sci. 288 (2014) 695–701. https://doi.org/10.1016/j.apsusc.2013.10.107.

[41] H. Yasuda, Y. Fujiwara, N. Mizuno, M. Misono, Oxidation of carbon monoxide on $LaMn_{1-x}Cu_xO_3$ perovskite-type mixed oxides, J. Chem. Soc. Faraday Trans. 90 (1994) 1183–1189. https://doi.org/10.1039/FT9949001183.

[42] J.H. Kim, J.T.S. Irvine, Characterization of layered perovskite oxides $NdBa_{1-x}Sr_xCo_2O_{5+\delta}$ (x = 0 and 0.5) as cathode materials for IT-SOFC, Int. J. Hydrogen Energy. 37 (2012) 5920–5929. https://doi.org/10.1016/j.ijhydene.2011.12.150.

[43] J.H. Kim, A. Manthiram, Layered $LnBaCo_2O_{5+\delta}$ perovskite cathodes for solid oxide fuel cells: An overview and perspective, J. Mater. Chem. A. 3 (2015) 24195–24210. https://doi.org/10.1039/c5ta06212h.

[44] L. Zhang, S. Li, T. Xia, L. Sun, L. Huo, H. Zhao, Co-deficient $PrBaCo_{2-x}O_{6-\delta}$ perovskites as cathode materials for intermediate-temperature solid oxide fuel cells: Enhanced electrochemical performance and oxygen reduction kinetics, Int. J. Hydrogen Energy. 43 (2018) 3761–3775. https://doi.org/10.1016/j.ijhydene.2018.01.018.

[45] J.S. PARK, H.G. KIM, Electrical Conductivity and Defect Models of MgO-Doped Cr_2O_3, J. Am. Ceram. Soc. 71 (1988) 173–176. https://doi.org/10.1111/j.1151-2916.1988.tb05024.x.

[46] K.E. Song, H. Schlegl, C.G. Kim, K.S. Baek, Y.R. Lim, J.H. Nam, H.S. Kim, J.H. Kim, Electrical conductivity properties of porous $SmBaCo_2O_{5+d}$ and $SmBa_{0.5}Sr_{0.5}Co_2O_{5+d}$ layered perovskite oxide systems for solid oxide fuel cell, Ceram. Int. 48 (2022) 28649–28658. https://doi.org/10.1016/j.ceramint.2022.06.179.

[47] K.E. Song, J.W. Lee, Y.R. Lim, S.W. Baek, T.H. Shin, S. Lee, H. Schlegl, J.H. Kim, Influence of microstructure and applied current on the electrical conductivity of $SmBaCo_2O_{5+d}$ cathode in solid oxide fuel cell, Int. J. Hydrogen Energy. 47 (2022) 15875−15886. https://doi.org/10.1016/j.ijhydene.2022.03.056.

[48] K.S. Baek, S.W. Baek, H. Kang, W. Choi, J.Y. Park, S. Saxin, S.K. Lee, J.H. Kim, Electrical conductivity characteristics of Sr substituted layered perovskite cathode ($SmBa_{0.5}Sr_{0.5}Co_2O_{5+d}$) for intermediate temperature-operating solid oxide fuel cell, Ceram. Int. 48 (2022) 15770–15779. https://doi.org/10.1016/j.ceramint.2022.02.114.

[49] K.E. Song, H. Schlegl, H. Kang, W. Choi, J.H. Kim, Electrochemical characteristic of non-stoichiometric $SmBa_{0.45}Sr_{0.5}Co_2O_{5+d}$ layered perovskite oxide system for IT-SOFC cathode, Int. J. Hydrogen Energy. 48 (2023) 17664–17676. https://doi.org/10.1016/j.ijhydene.2023.01.255.

[50] A. Aguadero, J.A. Alonso, S.J. Skinner, J. Kilner, A New Family of Mo-Doped $SrCoO_{3-d}$, Chem. Mater. 24 (2012) 2655–2663.

[51] J.H. Chan, J.A. Bock, H. Guo, S. Trolier-Mckinstry, C.A. Randall, High-temperature thermoelectric characterization of filled strontium barium niobates: Power factors and carrier concentrations, J. Mater. Res. 32 (2017) 1160–1167. https://doi.org/10.1557/jmr.2017.18.

Figure captions

Figure 1. X-ray diffraction (XRD) patterns of synthesized $SmBa_{0.5}Sr_{0.5}Co_xO_{5+d}$ (x = 1.9~2.1).

Figure 2. XRD patterns of (a) the composite of SBSCO-2.05 with CGO91, (b) SBSCO-2 with YSZ, (c) SBSCO-2.05 with YSZ, and (d) Characteristics of secondary phases in SBSCO-2 with YSZ and SBSCO-2.05 with YSZ.

Figure 3. TGA results of $SmBa_{0.5}Sr_{0.5}Co_xO_{5+d}$ (x = 1.9~2.1). (a) Thermogravimetric results with increasing temperature, and (b) temperature dependent decrease in oxygen content.

Figure 4. (a) ASR of $SmBa_{0.5}Sr_{0.5}Co_xO_{5+d}$ (x = 1.9~2.1) and of the composite cathode of SBSCO-2.05 with CGO91, (b) Nyquist plots of the impedance of SBSCO-2.05.

Figure 5. Oxygen spectra of (a) SBSCO-2 and (b) SBSCO-2.05, and cobalt spectra of (c) SBSCO-2 and (d) SBSCO-2.05.

Figure 6. (a~e) Electrical conductivities of dense $SmBa_{0.5}Sr_{0.5}Co_xO_{5+d}$ (x = 1.9~2.1) and (f) Total electrical conductivities of $SmBa_{0.5}Sr_{0.5}Co_xO_{5+d}$ (x = 1.9~2.1) with respect to various amounts of Co at the perovskite B-site.

Figure 7. Electrical conductivities of the porous-type SBSCO-2.05 cathode: conductivity results under applied current (a) in an air atmosphere, (b) in a N_2 atmosphere, and (c) in air and N_2 with an applied current of 0.05 A.

Table captions

Table 1. Relative intensity of the secondary phase peaks in a composite of SBSCO-2 with YSZ and SBSCO-2.05 with YSZ.

Table 2. Oxygen contents and d values of $SmBa_{0.5}Sr_{0.5}Co_xO_{5+d}$ (x = 1.9~2.1).

Table 3. ASR results for $SmBa_{0.5}Sr_{0.5}Co_xO_{5+d}$ (x = 1.9~2.1).

Table 4. Summarized results R_1 and R_2 of the SBSCO-2.05 cathode.

Table 5. The results of the O_{1s} spectra for SBSCO-2 and SBSCO-2.05.

Table 6. The results of the Co_{2p} spectra for SBSCO-2 and SBSCO-2.05.

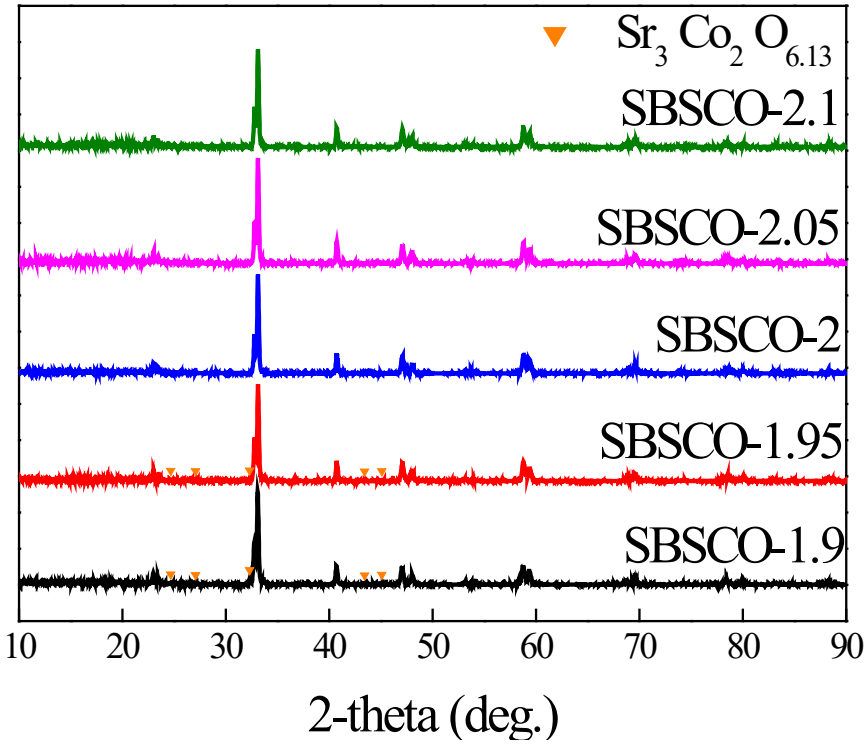

Fig 1. X-ray diffraction (XRD) patterns of synthesized $SmBa_{0.5}Sr_{0.5}Co_xO_{5+d}$ (x = 1.9~2.1).

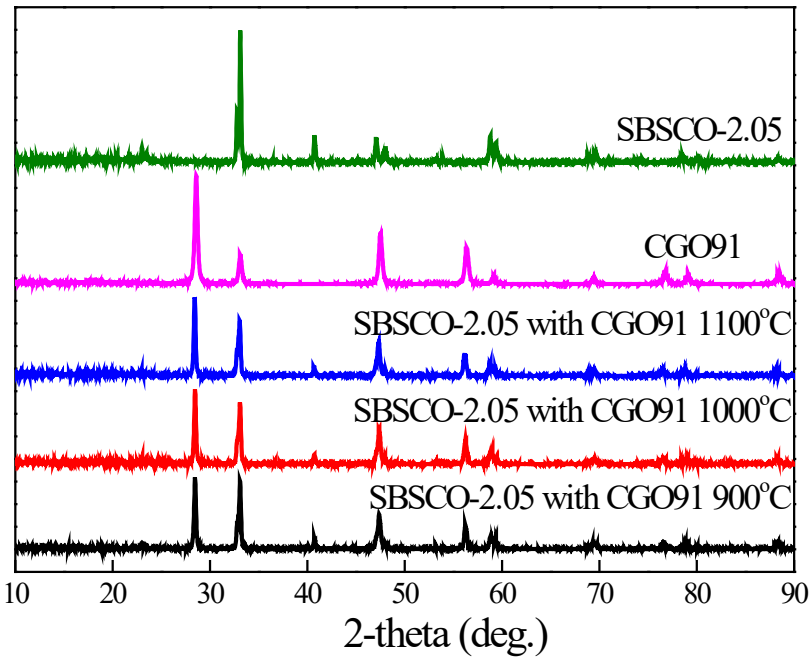
SBSCO-2.05
CGO91
SBSCO-2.05 with CGO91 1100°C
SBSCO-2.05 with CGO91 1000°C
SBSCO-2.05 with CGO91 900°C
10
20
30
40
50
60
70
80
90
2-theta (deg.)

(a)

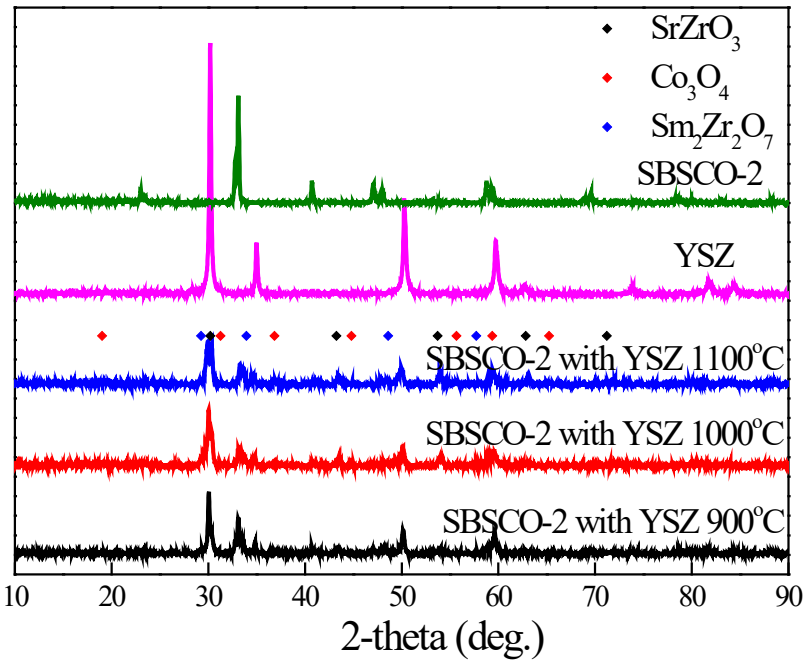
SrZrO3
Co3O4
Sm2Zr2O7
SBSCO-2
YSZ
SBSCO-2 with YSZ 1100°C
SBSCO-2 with YSZ 1000°C
SBSCO-2 with YSZ 900°C
10
20
30
40
50
60
70
80
90
2-theta (deg.)

(b)

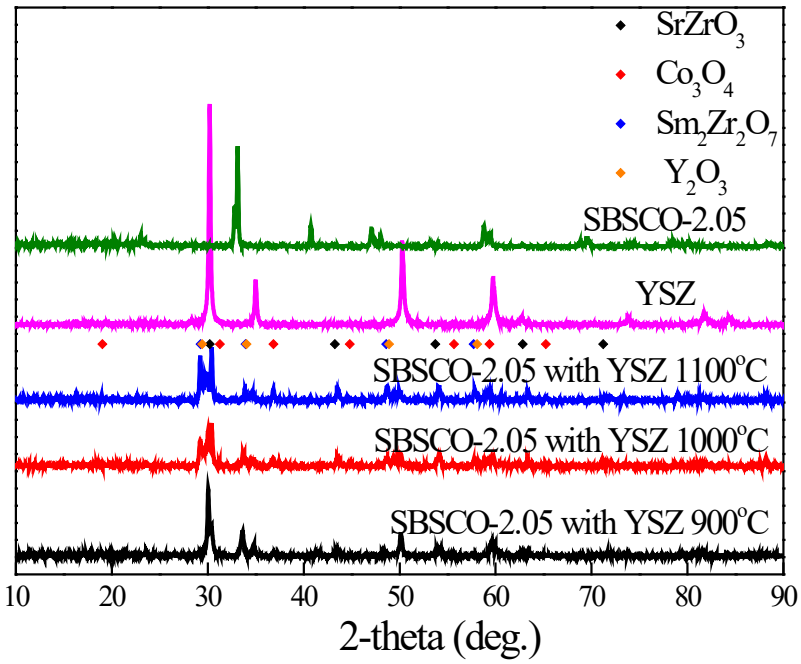
SrZrO3
Co3O4
Sm2Zr2O7
Y2O3
SBSCO-2.05
YSZ
SBSCO-2.05 with YSZ 1100°C
SBSCO-2.05 with YSZ 1000°C
SBSCO-2.05 with YSZ 900°C
10
20
30
40
50
60
70
80
90
2-theta (deg.)

(c)

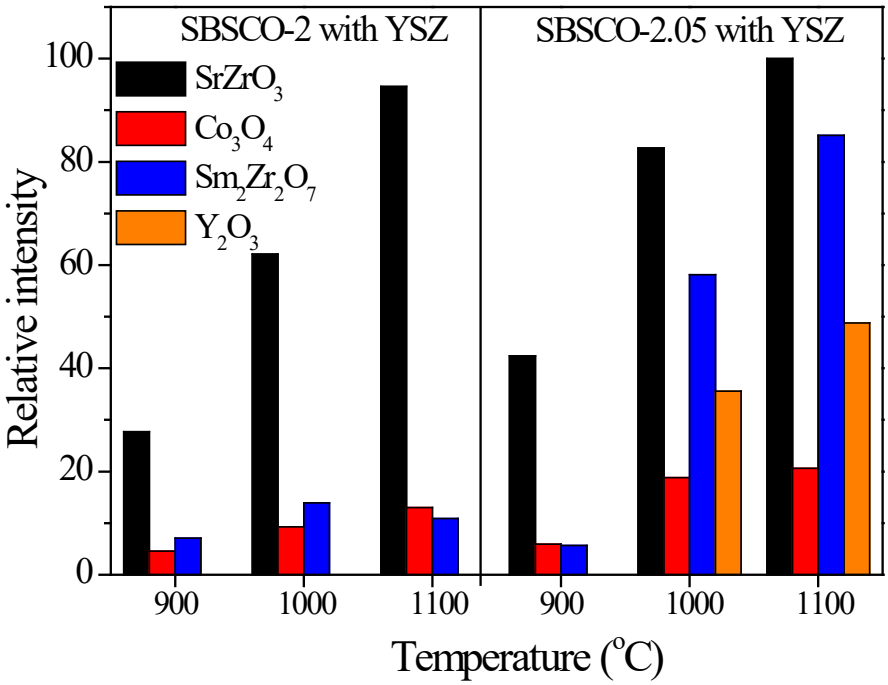

(d)

Fig 2. XRD patterns of (a) the composite of SBSCO-2.05 with CGO91, (b) SBSCO-2 with YSZ, (c) SBSCO-2.05 with YSZ, and (d) Characteristics of secondary phases in SBSCO-2 with YSZ and SBSCO-2.05 with YSZ.

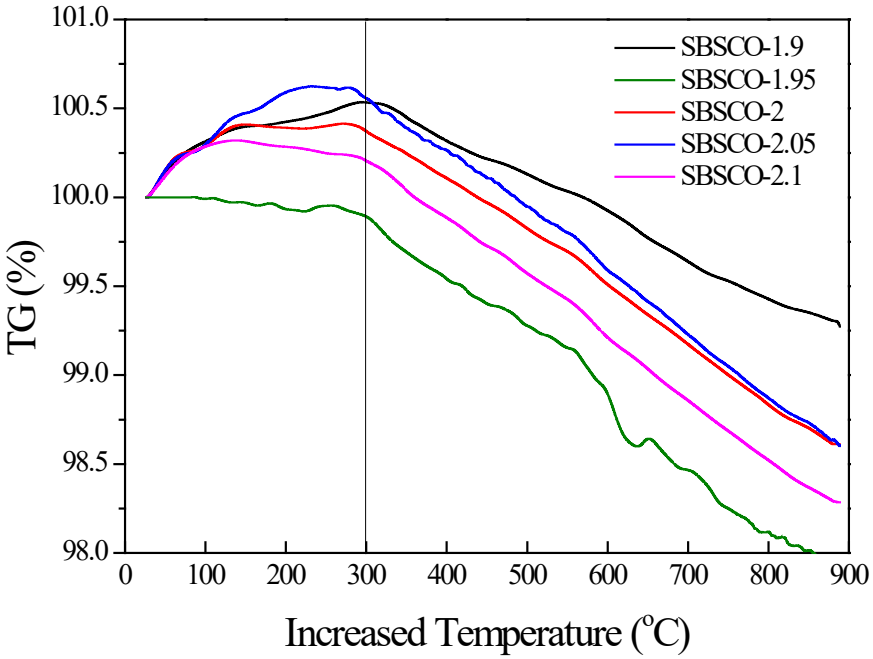
101.0
100.5
100.0
99.5
99.0
98.5
98.0
TG (%)
0
100
200
300
400
500
600
700
800
900
Increased Temperature (°C)
SBSCO-1.9
SBSCO-1.95
SBSCO-2
SBSCO-2.05
SBSCO-2.1

(a)

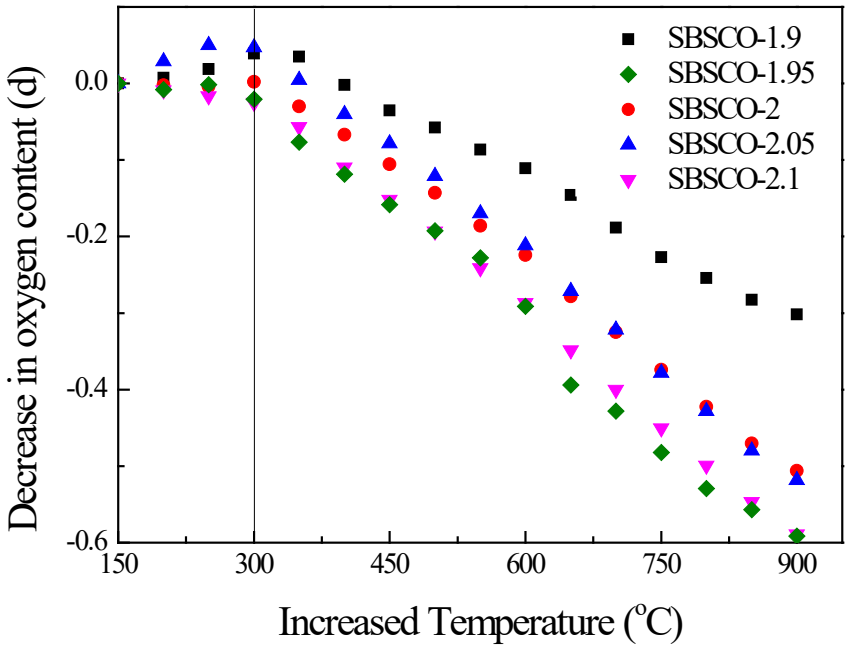

(b)

Fig 3. TGA results of $SmBa_{0.5}Sr_{0.5}Co_xO_{5+d}$ (x = 1.9~2.1). (a) Thermogravimetric results with increasing temperature, and (b) temperature dependent decrease in oxygen content.

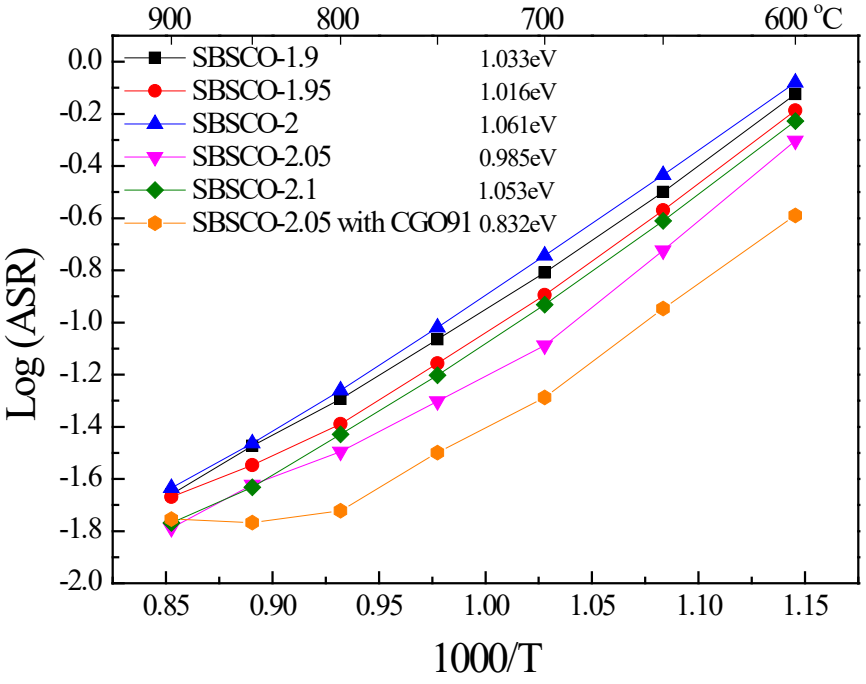
900
800
700
600 °C
SBSCO-1.9 1.033eV
SBSCO-1.95 1.016eV
SBSCO-2 1.061eV
SBSCO-2.05 0.985eV
SBSCO-2.1 1.053eV
SBSCO-2.05 with CGO91 0.832eV
Log (ASR)
1000/T

(a)

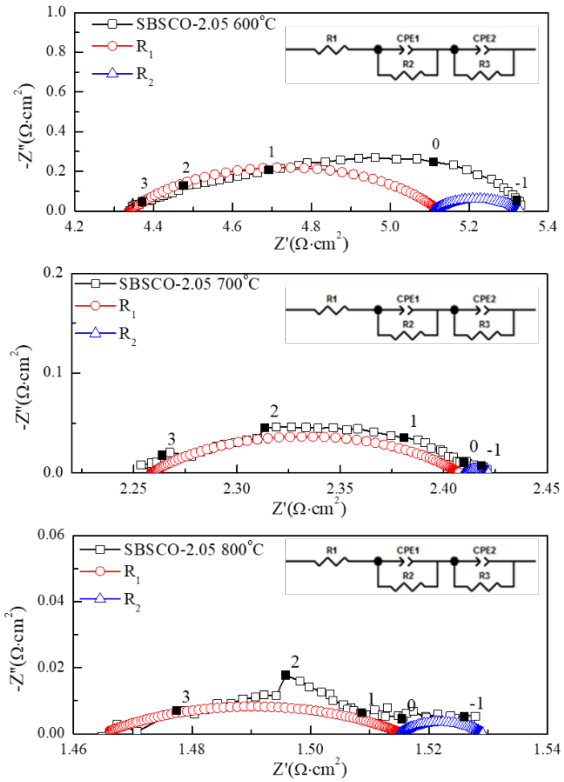
SBSCO-2.05 600°C
SBSCO-2.05 700°C
SBSCO-2.05 800°C
R1
CPE1
CPE2
R2
R3
-Z''(Ω·cm²)
Z'(Ω·cm²)

(b)

Fig 4. (a) ASR of $SmBa_{0.5}Sr_{0.5}Co_xO_{5+d}$ (x = 1.9~2.1) and of the composite cathode of SBSCO-2.05 with CGO91, (b) Nyquist plots of the impedance of SBSCO-2.05

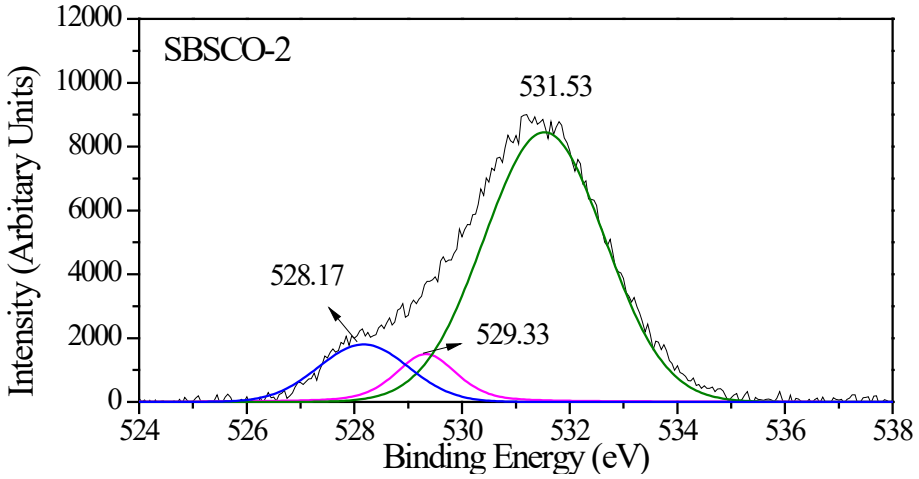
SBSCO-2
531.53
528.17
529.33
Intensity (Arbitary Units)
Binding Energy (eV)
12000
10000
8000
6000
4000
2000
0
524
526
528
530
532
534
536
538

(a)

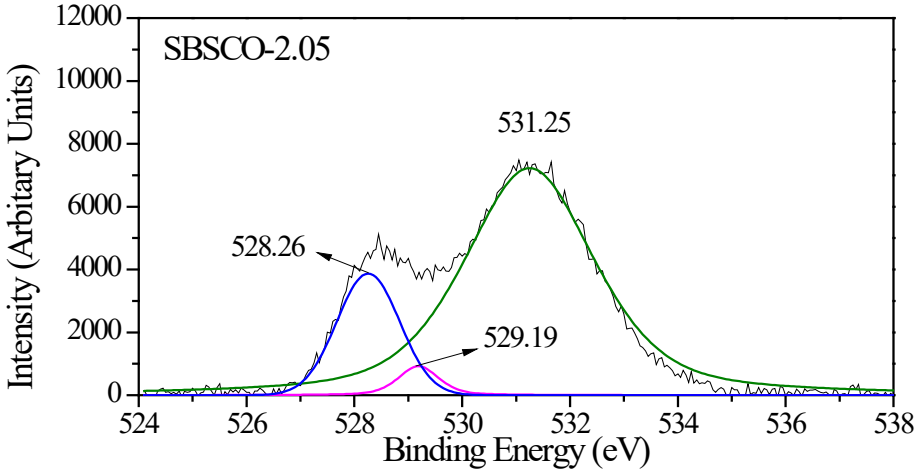
SBSCO-2.05
531.25
528.26
529.19
Intensity (Arbitary Units)
Binding Energy (eV)
12000
10000
8000
6000
4000
2000
0
524
526
528
530
532
534
536
538

(b)

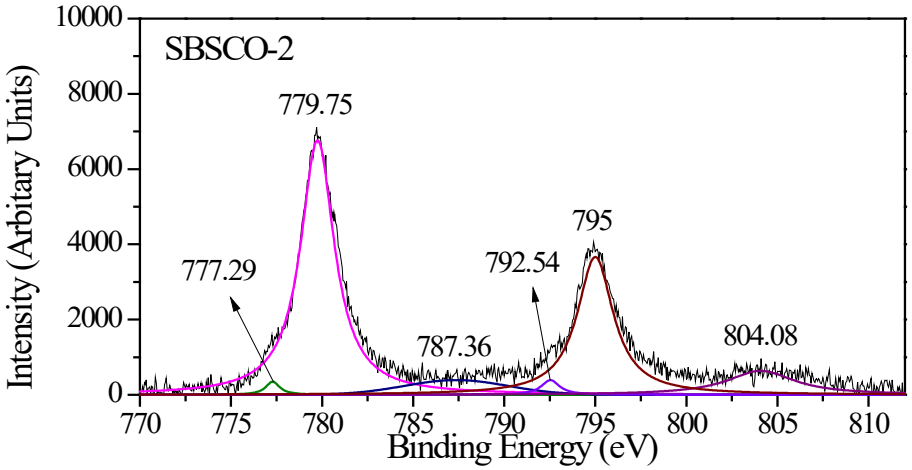

(c)

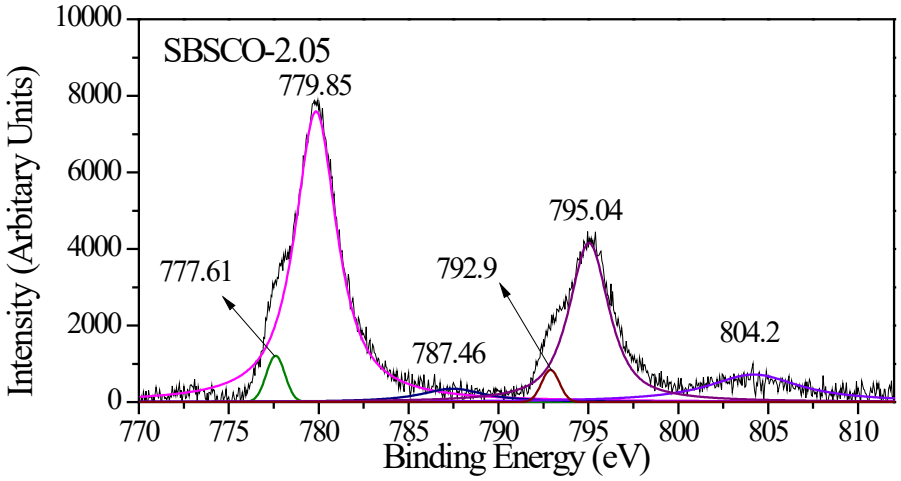

(d)

Fig 5. Oxygen spectra of (a) SBSCO-2 and (b) SBSCO-2.05, and cobalt spectra of (c) SBSCO-2 and (d) SBSCO-2.05.

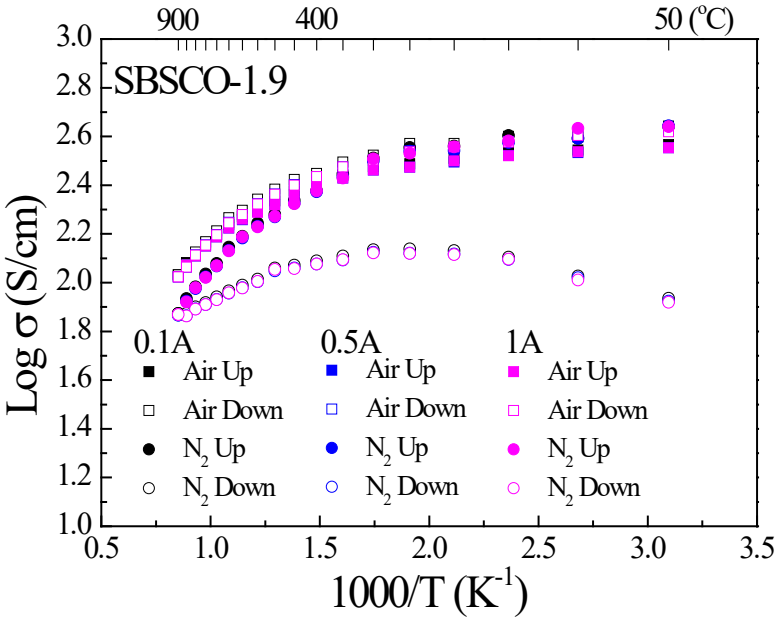
900
400
50 (°C)
SBSCO-1.9
Log σ (S/cm)
1000/T (K-1)
0.1A
0.5A
1A
Air Up
Air Down
N2 Up
N2 Down

(a)

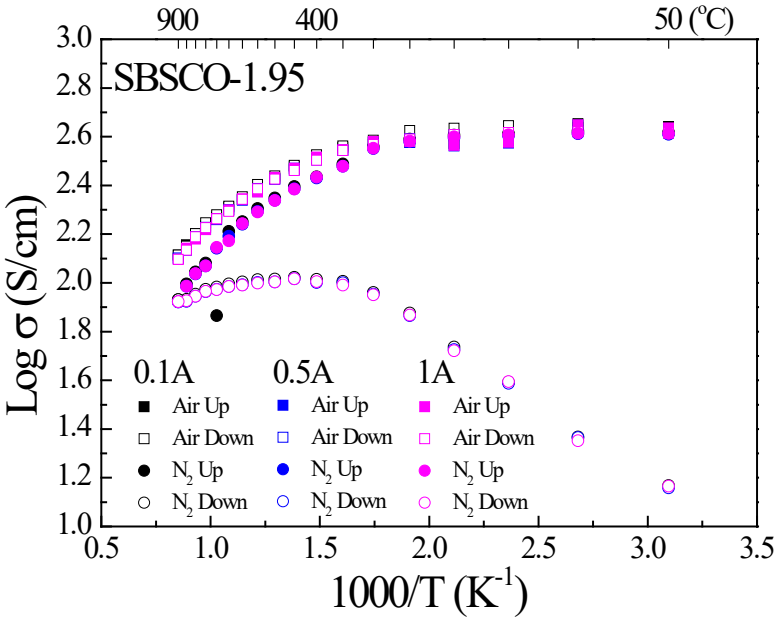
900
400
50 (°C)
SBSCO-1.95
Log σ (S/cm)
1000/T (K-1)
0.1A
0.5A
1A
Air Up
Air Down
N2 Up
N2 Down

(b)

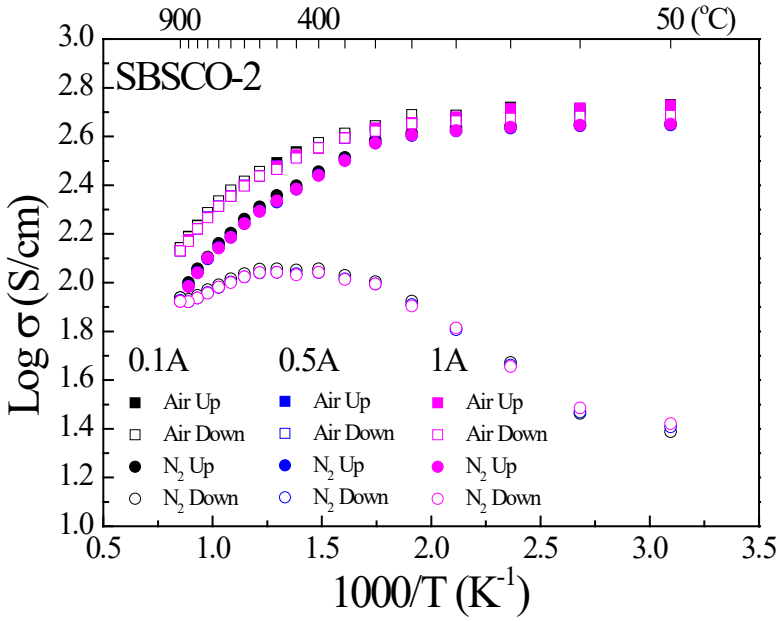
900
400
50 (°C)
SBSCO-2
Log σ (S/cm)
1000/T (K-1)
0.1A
0.5A
1A
Air Up
Air Down
N2 Up
N2 Down

(c)

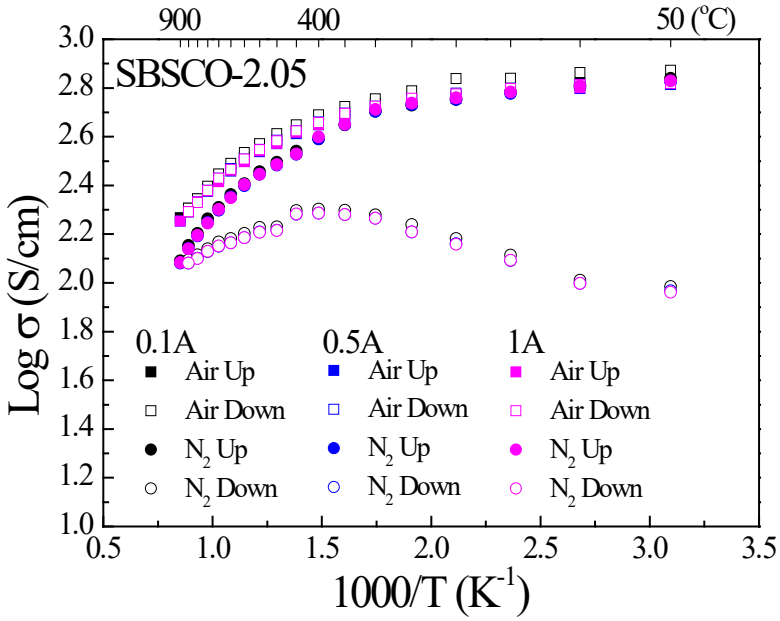
900
400
50 (°C)
SBSCO-2.05
Log σ (S/cm)
1000/T (K-1)
0.1A
0.5A
1A
Air Up
Air Down
N2 Up
N2 Down

(d)

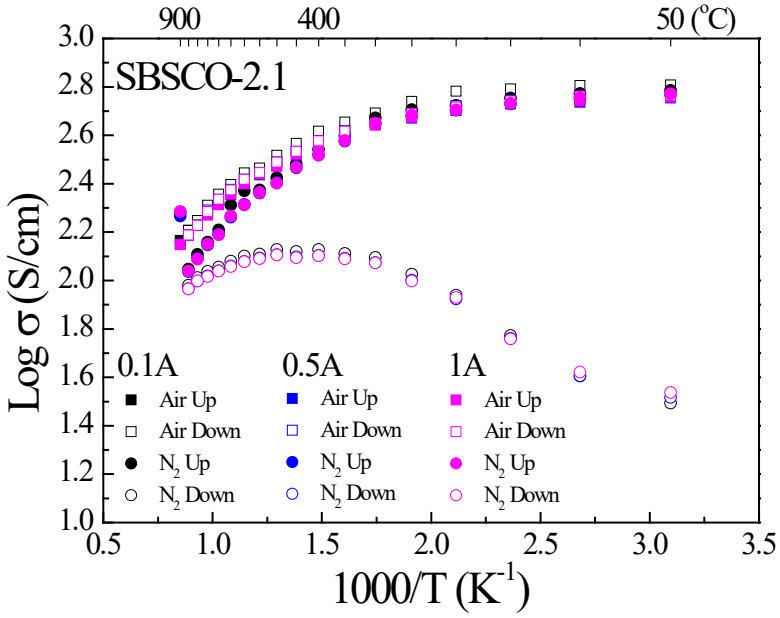

(e)

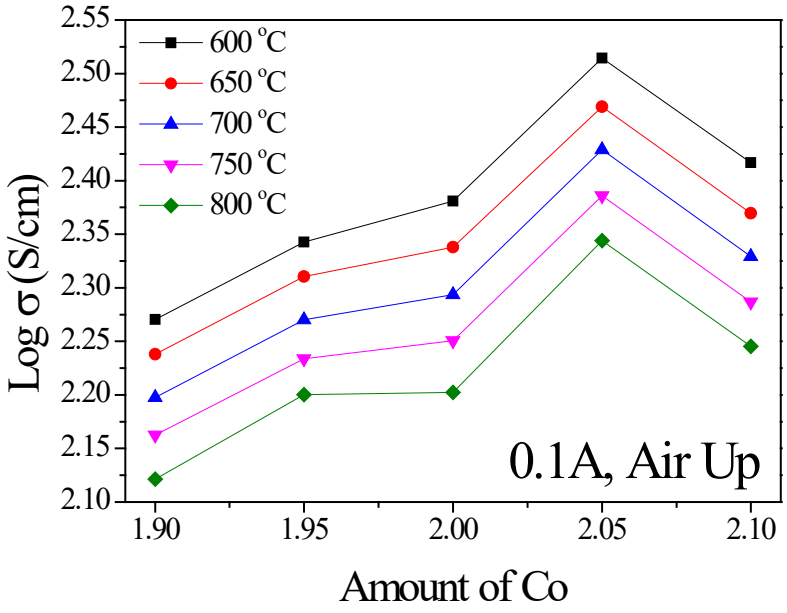

(f)

Fig 6. (a~e) Electrical conductivities of dense $SmBa_{0.5}Sr_{0.5}Co_xO_{5+d}$ (x = 1.9~2.1) and (f) Total electrical conductivities of $SmBa_{0.5}Sr_{0.5}Co_xO_{5+d}$ (x = 1.9~2.1) with respect to various amounts of Co at the perovskite B-site.

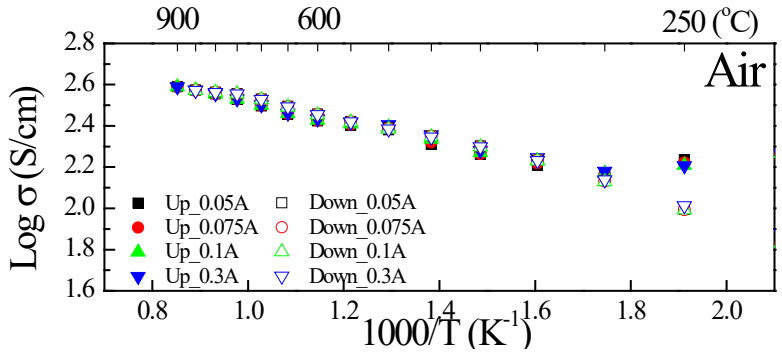
900
600
250 (°C)
Air
Log σ (S/cm)
2.8
2.6
2.4
2.2
2.0
1.8
1.6
Up_0.05A
Up_0.075A
Up_0.1A
Up_0.3A
Down_0.05A
Down_0.075A
Down_0.1A
Down_0.3A
0.8
1.0
1.2
1.4
1.6
1.8
2.0
1000/T (K-1)

(a)

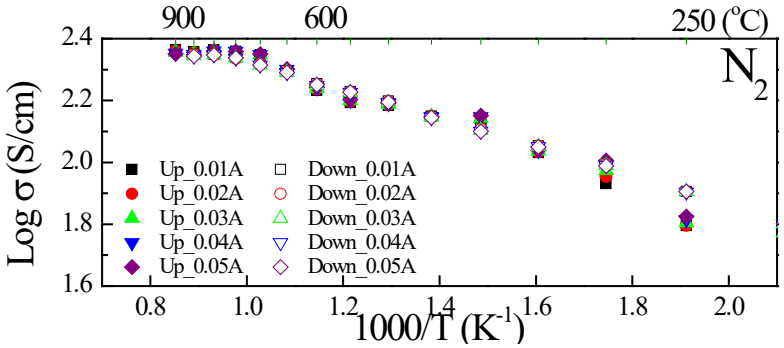
900
600
250 (°C)
N2
Log σ (S/cm)
2.4
2.2
2.0
1.8
1.6
Up_0.01A
Up_0.02A
Up_0.03A
Up_0.04A
Up_0.05A
Down_0.01A
Down_0.02A
Down_0.03A
Down_0.04A
Down_0.05A
0.8
1.0
1.2
1.4
1.6
1.8
2.0
1000/T (K-1)

(b)

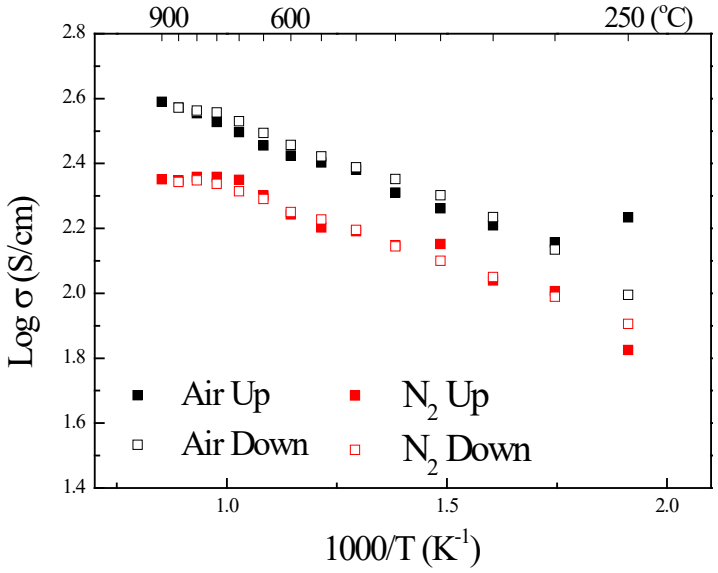

(c)

Fig 7. Electrical conductivities of the porous-type SBSCO-2.05 cathode: conductivity results under applied current (a) in an air atmosphere, (b) in a N_2 atmosphere, and (c) in air and N_2 with an applied current of 0.05 A.

Table 1. Relative intensity of the secondary phase peaks in a composite of SBSCO-2 with YSZ and SBSCO-2.05 with YSZ.

		Relative intensity (%)			
	Temperature (ºC)	$SrZrO_3$	Co_3O_4	$Sm_2Zr_2O_7$	Y_2O_3
SBSCO-2 with YSZ	900	27.7	4.6	7.1	-
	1000	62.1	9.3	13.9	-
	1100	94.6	13	10.9	-
SBSCO-2.05 with YSZ	900	42.4	5.9	5.7	-
	1000	82.7	18.8	58.1	35.6
	1100	100	20.6	85.1	48.8

Table 2. Oxygen contents and d values of $SmBa_{0.5}Sr_{0.5}Co_xO_{5+d}$ (x = 1.9~2.1).

	SBSCO-1.9	SBSCO-1.95	SBSCO-2	SBSCO-2.05	SBSCO-2.1
Oxygen contents at RT	5.35	5.425	5.5	5.575	5.65
d values at 900 ºC	-0.30	-0.59	-0.51	-0.52	-0.59
Oxygen contents at 900 ºC	5.05	4.835	4.99	5.055	5.06

Table 3. ASR results for $SmBa_{0.5}Sr_{0.5}Co_xO_{5+d}$ (x = 1.9~2.1).

	ASR of various composition ($\Omega \cdot cm^2$)				
Temperature(°C)	SBSCO-1.9	SBSCO-1.95	SBSCO-2	SBSCO-2.05	SBSCO-2.1
600	0.7515	0.6513	0.8331	0.4990	0.5930
650	0.3167	0.2691	0.3683	0.1893	0.2452
700	0.1555	0.1274	0.1806	0.0818	0.1170
750	0.0861	0.0697	0.0958	0.0499	0.0628
800	0.0509	0.0407	0.0549	0.0320	0.0373
850	0.0336	0.0283	0.0344	0.0239	0.0233
900	0.0219	0.0214	0.0232	0.0163	0.0170

Table 4. Summarized results R_1 and R_2 of the SBSCO-2.05 cathode.

	ASR of SBSCO-2.05 ($\Omega \cdot cm^2$)	
Temperature (°C)	R_1	R_2
600	0.385	0.114
650	0.175	0.014
700	0.076	0.006
750	0.041	0.009
800	0.025	0.006
850	0.017	0.006
900	0.009	0.007

Table 5. The results of the O_{1s} spectra for SBSCO-2 and SBSCO-2.05.

		SBSCO-2	SBSCO-2.05
LBE	BE (eV)	528.17	528.26
	Area (%)	12.55	16.75
IBE	BE (eV)	529.33	529.19
	Area (%)	8.48	3.06
HBE	BE (eV)	531.23	531.25
	Area (%)	78.96	80.19

Table 6. The results of the Co_{2p} spectra for SBSCO-2 and SBSCO-2.05.

		SBSCO-2	SBSCO-2.05
Co $2p_{3/2}$	BE (eV)	779.75	779.85
	Area (%)	51.70	53.64
Co^{2+}, Co^{4+}	BE (eV)	787.36	787.46
	Area (%)	6.03	3.9
Co $2p_{1/2}$	BE (eV)	795	795.04
	Area (%)	29.84	26.49
Co^{3+}, Co^{4+}	BE (eV)	804.08	804.2
	Area (%)	9.76	11.66